Hydrogen Production via Solar-Aided Water Splitting Thermochemical Cycles with Nickel Ferrite: Experiments and Modeling

Christos Agrafiotis, Alexandra Zygogianni, and Chrysoula Pagkoura
Aerosol and Particle Technology Laboratory (APTL), Chemical Process Engineering Research Institute, Center for Research and Technology-Hellas (CERTH/CPERI), P.O. Box 361, 57001, Thermi - Thessaloniki, Greece

Margaritis Kostoglou
Dept. of Chemistry, Aristotle University of Thessaloniki, Univ. Box 116, Thessaloniki 54124, Greece

Athanasios G. Konstandopoulos
Aerosol and Particle Technology Laboratory (APTL), Chemical Process Engineering Research Institute, Center for Research and Technology-Hellas (CERTH/CPERI), P.O. Box 361, 57001, Thermi - Thessaloniki, Greece

Dept. of Chemical Engineering, Aristotle University of Thessaloniki, P.O. Box 1517, 54006, Thessaloniki, Greece

DOI 10.1002/aic.13882
Published online August 28, 2012 in Wiley Online Library (wileyonlinelibrary.com).

Water splitting — thermal reduction cyclic studies with $NiFe_2O_4$ redox materials were performed in a differential fixed-bed laboratory reactor in the temperature range 700–1,400°C to quantify the effects of operation temperatures and steam mole fraction on hydrogen and oxygen yields. Hydrogen yield increased drastically by an increase of the water splitting temperature from 800 to 1,000°C reaching a plateau at 1,100°C. In parallel, a simple mathematical model was formulated describing the water splitting process via the heterogeneous surface reactions of water vapor with the redox powder material, from which, in conjunction to the aforementioned experiments, the kinetic parameters of the water splitting and thermal reduction reactions were extracted. The water splitting kinetic constants exhibited weak temperature dependence between 700 and 1,100°C suggesting the existence on the redox material of more than one type of oxygen storage sites with respect to ease of exposure and accessibility to the gas phase. © 2012 American Institute of Chemical Engineers *AIChE J,* 59: 1213–1225, 2013
Keywords: thermochemical cycles, nickel ferrite, solar hydrogen, water splitting, thermal reduction

Introduction

Thermochemical cycles are multistep processes where water is decomposed into hydrogen and oxygen via two or more chemical reactions that form a closed cycle. The redox-pair-based thermochemical cycles in particular, are comprised by two reactions, the thermal reduction/TR (regeneration) and the water splitting/WS reaction, in general described as follows

$$MO_{ox} \rightarrow MO_{red} + {}^1/_2O_2(g) \quad (1)$$

$$MO_{red} + H_2O\,(g) \rightarrow MO_{ox} + H_2(g) \quad (2)$$

The oxidized form of the redox material MO_{ox} is usually the higher-valence oxide of a metal exhibiting multiple oxidation states. During the first, higher-temperature step (TR) this oxidized form releases a quantity of oxygen and transforms to its reduced (lower-valence) state. During the second (WS) step the reduced material is oxidized back to the higher-valence one by taking oxygen from water and producing hydrogen, establishing, thus, a cyclic process.

Solar-aided hydrogen production via water splitting through thermochemical cycles is based on the use of concentrated solar radiation as the energy source for performing the high-temperature endothermic reactions of the cycle. Direct solar irradiation can be concentrated and collected by a range of concentrating solar power (CSP) technologies to provide medium-to-high temperature heat. Therefore, the effective conversion of the huge energy potential of solar radiation to chemical energy carriers such as hydrogen is of primary technological interest.[1]

Current engineering challenges in the field of thermochemical cycles' "solar chemistry" include synthesis of active redox materials as well as design and operation of novel receiver/reactor systems capable to collect effectively the concentrated solar radiation, and at the same time to perform in an efficient and elegant manner the high-temperature reactions mentioned previously. Despite early extensive research with respect to synthesis and evaluation of active

Correspondence concerning this article should be addressed to C. Agrafiotis, Deutsches Zentrum für Luft- und Raumfahrt (DLR), German Aerospace Center, Institute of Solar Research, Solar Chemical Engineering, Linder Höhe, 51147 Koeln, Germany at Christos.Agrafiotis@dir.de and A. G. Konstandopoulos at agk@cperi.certh.gr.

redox pair materials, solar reactor concepts have only been reported in the literature much later with the first ones being rotating cavity reactors targeted to the solar thermal reduction of ZnO to Zn.[2,3] The HYDROSOL research group (including among others the present authors) has introduced the concept of monolithic, honeycomb solar reactors for performing these redox pair cycles for the production of hydrogen from the splitting of steam using solar energy.[4,5] The reactor, inspired from the well-known automobile catalytic converters,[6] is based on the incorporation of active redox pair powders as coatings on multichannelled monolithic honeycomb structures capable of achieving and sustaining high temperatures when irradiated with concentrated solar irradiation.[7] When steam passes through the solar reactor, the coating material splits water vapor by "trapping" its oxygen and leaving in the effluent gas stream pure hydrogen. In a subsequent step the oxygen-"trapping" coating is thermally reduced (regenerated) by increasing the amount of solar heat absorbed by the reactor. Several other solar reactor types have been subsequently proposed like rotary-cylinders,[8] spouted powder beds[9,10] and counter-rotating-rings.[11,12] A modular, dual-chamber,[13,14] redox-material-coated-honeycomb HYDROSOL reactor has been scaled-up to the 100 kW level, coupled on a solar tower facility (Plataforma Solar de Almeria, Spain) and achieved continuous solar-operated water splitting—regeneration cycles demonstrating the "proof-of-concept" of the proposed design.[15] For an efficient further scale-up of such reactors, although, parameters such as the reactor volume and the loading with the redox coating required have to be optimized by modeling and simulations, taking into account the solar flux and the resulting temperature distribution, the heat-transfer characteristics, the reaction rates and transient phenomena due to reactor operation at alternating solar flux conditions. Even though the problem of modeling the transient operation of monolithic reactors has been studied extensively mainly in the context of automotive catalytic converters[16,17] solar reactors have their own distinct features different than those of automotive converters. At first the much higher temperatures needed for the two reactions bring into play the radiation heat-transfer mechanism which can be ignored for temperatures lower than 600°C encountered in automotive converters.[18] In addition, the large temperature differences developed between wall and gas in the channel sets into question the perimeter averaged equations for the channels and the use of heat-transfer coefficients. Since the concept of monolithic honeycomb solar hydrogen reactors is relatively recent, only few modeling approaches can be found in the literature such as a single perimeter average model[14] and a two-dimensional (2-D) pseudo-homogeneous model of the whole monolith using the library Modelica.[19,20] Any such model needs specific values for the kinetic constants of the reactions which can be found by performing isothermal experiments in differential laboratory reactors. In a recent work by some of the present authors,[21] a discussion of the modeling aspects of the honeycomb reactor for solar hydrogen production was presented and indicative results were shown to stress several aspects of the process. These results were obtained by employing water splitting kinetic constants computed from experimental data obtained in packed-bed reactors with the redox material in powder form;[22] however, these experimental results were on the one hand limited within a narrow temperature range, and on the other hand, did not include the thermal reduction step for which the respective data were obtained by fitting experimental results from monolithic reactors.

Based on the results of a recent work by the authors[23] this work has a two-fold target. One objective is the optimization of the water splitting—thermal reduction performance of a "model redox material system" in the actual solar operation range via a systematic parametric investigation of the process. An equally important objective is to develop reliable reaction models and determine the reactions' kinetic constants to accurately simulate the operation of such honeycomb solar hydrogen production reactors. Even though many ferrite compositions have been extensively tested for the particular applications,[9,10,12,24–27] in several cases their synthesis and characterization conditions (temperature, atmosphere) are much milder than those during the subsequently performed water splitting—thermal reduction cyclic operation. As a result, phenomena associated with the calcination of the ferrite material at higher-than-the-synthesis-temperatures (e.g., burnout of possible reminiscent organic precursor materials, reduction of surface area, alteration/collapse of porous structure etc.) overlap with the chemical reactions during thermochemical cyclic operation. In other cases, testing conditions are not representative of those during the actually targeted operation. For instance, in several cases reduction before water splitting takes place with chemical rather than thermal-only means; as a result the extent of reduction can be higher than that to be encountered during actual operation—for example, a quantity of metal can coexist with the reduced form of the oxide. Such facts make hard to distinguish between competing effects and to propose appropriate reaction mechanisms or extract reliable water splitting—thermal reduction kinetic data. With this rationale, in a previous work by the present authors, a variety of redox materials were synthesized and then calcined under air and under nitrogen at 1,400°C to establish a common background for relevant comparisons.[23] It was found—and corroborated by other studies reported in the literature[24–27]—that among the many ferrite materials tested for the targeted application, Zn-containing ones exhibit Zn-volatilization problems and Mn-containing ones phase stability problems under air atmosphere at high temperatures. These facts practically leave only $NiFe_2O_4$ and $CoFe_2O_4$ as the most "robust" among the ferrites, capable to operate reliably at the real conditions of a solar-aided process. Between these two, $NiFe_2O_4$ was the first material selected as a "model system" for a thorough parametric study of the water splitting—thermal reduction reactions to quantify the effects of various operating parameters presented in this work, primarily due to its extensive use in such applications.[10,25–28]

Experimental

In particular, the $NiFe_2O_4$ material synthesized by solid-phase self-propagating high-temperature synthesis was employed (denoted, hereafter, as SHS $NiFe_2O_4$), due to the amenability of this route for the synthesis of large material quantities. Few comparative experiments at particular cycle conditions were also performed with a $NiFe_2O_4$ synthesized via solid-state synthesis (denoted, hereafter, as SSS $NiFe_2O_4$)[23] from the co-firing of the respective single-metal oxides (NiO and Fe_2O_3).

The parametric thermal reduction—water splitting experiments were performed in a laboratory test rig consisting of a 20 mm dia. alumina tubular reactor enclosed within a high-

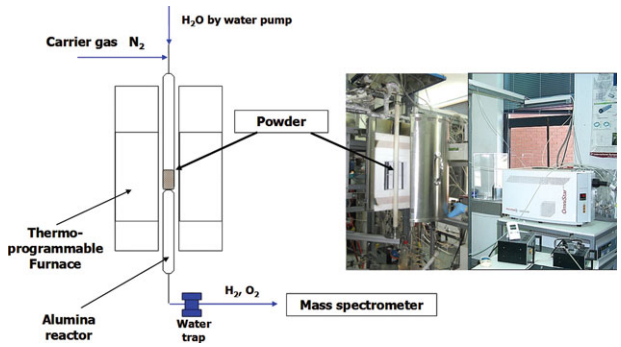

Figure 1. Schematic (left), and actual (right) test rig for water splitting—thermal reduction experiments.

[Color figure can be viewed in the online issue, which is available at wileyonlinelibrary.com.]

temperature programmable furnace (Thermcraft, Inc.) capable of reaching temperatures of 1,500°C (Figure 1). A quantity of 10 g of the redox material powder to be tested was placed in the middle of the reactor forming a bed of approximately 1 cm height supported by quartz wool. The first step—denoted, hereafter, as "activation"—involved heating of the powder under nitrogen with a flow rate of 2 lt/min, with a ramp of 15°C/min up to a certain temperature; in the particular study activation temperatures of 1,250, 1,320 and 1,400°C were tested. The dwell time at the activation temperature was also varied. Subsequently, the material was cooled under nitrogen to the desired water splitting temperature level; in this study water splitting temperatures of 700, 800 1,000 and 1,100°C were tested. When the targeted temperature level was reached, steam was introduced to the reactor in the nitrogen stream (mole fractions of steam tested were 8, 16 and 32%) flowing continuously over the heated sample with the aid of a manometric water pump and a heated evaporation line. The mole fractions of steam were calculated by converting the liquid water flow rate from the pump to moles of gaseous water vapor. After a particular dwell time at the water splitting temperature, the steam flow was switched off and the reactor was heated again with the same ramp of 15°C/min to the TR temperature level under pure nitrogen where it remained for a preset time. This WS—TR procedure was repeated once more, thus, all experiments involved an initial activation step under nitrogen and two subsequent WS—TR cycles. During the whole process the effluent, after passing through a water trap, was diverted to a mass spectrometer (Pfeiffer, Omnistar) via which hydrogen and oxygen concentrations were constantly monitored and recorded. The quantities of hydrogen and oxygen produced were calculated based on the areas of the corresponding mass spectrometer (MS) peaks. In all cyclic experiments the TR temperature was set equal to the initial activation temperature, so in the manuscript these two terms have the same meaning. After the end of the cyclic experiments (with the last step always being the TR one) the reactor was cooled down under nitrogen atmosphere, and the redox materials were collected for *ex situ* structural characterization by X-ray diffraction analysis (XRD) using a Siemens D-500 Kristalloflex X-ray powder diffractometer (Cu Kα radiation).

Due to the much higher redox material amounts used in this study in contrast to experiments reported in previous works, water splitting and thermal reduction experiments did not last until hydrogen/oxygen, respectively could not be further detected in the effluent stream but the activation/water splitting/thermal reduction times were initially kept constant at 30 min. This time was subsequently varied according to the experimental findings.

Results and Discussion

Water splitting—thermal reduction experiments

Effect of Water Splitting Temperature. The first set of the study involved experiments to quantify the effect of water splitting temperature on the hydrogen and oxygen yields. This effect is shown in Figure 2 for the SHS $NiFe_2O_4$, for four WS temperatures 700, 800 1,000 and 1,100°C, a constant TR temperature of 1,400°C, a steam mole fraction of 8% and a dwell time at all steps equal to 30 min. Throughout this work, hydrogen and oxygen concentrations are reported as "mmol of gas produced per g of redox material employed" and the gas concentration scale is the same for all experimental runs shown together on each figure. It can be seen that the amount of hydrogen produced increases with increasing water splitting temperature seeming although to reach a "plateau" value for temperatures higher than 1,000°C. The hydrogen and oxygen concentration evolution profiles seem to have a constant, self-similar shape regardless of the step and the temperature, especially for WS temperatures higher than 1,000°C. The only discrepancy in the oxygen profiles is the sharp first oxygen peak at the first TR step in the experiment with a WS temperature of 800°C. This is due to the fact that in the course of the experimental procedure at this WS temperature, after the first WS step (marked in the graph of Figure 2) the material was taken out of the test rig, ground in a mortar, and, thus, returned. This resulted in an abrupt initial peak of the oxygen concentration produced in the next step, indicating that at least some further sintering of the material takes place at the high-activation temperature levels employed and deteriorates the materials performance decreasing the gas product yield; this effect of sintering is alleviated by grinding.

Both the hydrogen and oxygen concentration profiles exhibit a maximum at the beginning and a gradual decay, thereafter, but the hydrogen ones are much sharper indicating that the WS reaction takes place much faster than the TR one. Since portions of the same initial batch of $NiFe_2O_4$

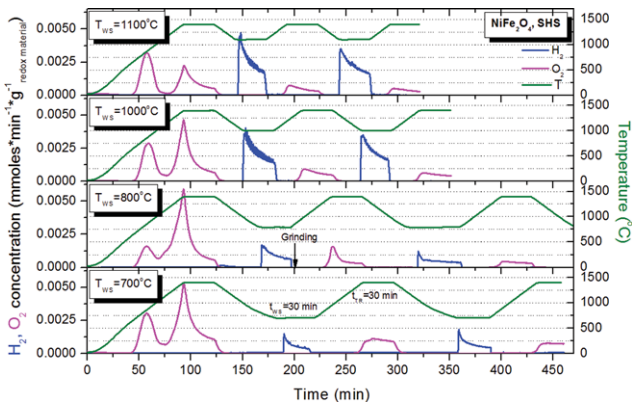

Figure 2. Effect of water splitting temperature on hydrogen and oxygen concentration for SHS $NiFe_2O_4$ for thermal reduction temperature = 1,400°C.

[Color figure can be viewed in the online issue, which is available at wileyonlinelibrary.com.]

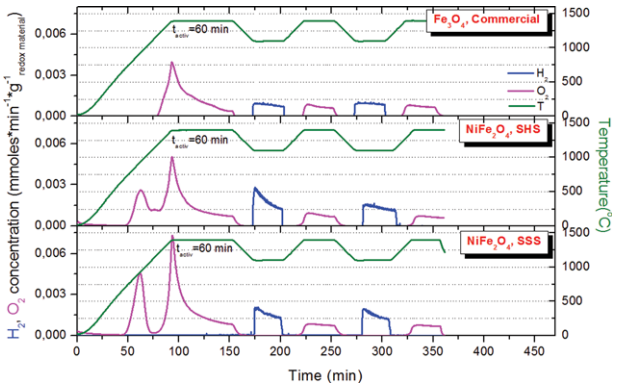

Figure 3. Comparison among $NiFe_2O_4$ synthesized via different routes and commercial Fe_3O_4 for thermal reduction temperature 1,400°C and water splitting temperature 1,100°C.

[Color figure can be viewed in the online issue, which is available at wileyonlinelibrary.com.]

material were used in all four experiments depicted in Figure 2, the relative peak height differences among the four oxygen evolution curves during the initial activation step should be attributed to small differences in the material batch used for each experiment.

Effect of Ni cation and of redox material synthesis route

The $NiFe_2O_4$ synthesized by SHS was compared to the SSS $NiFe_2O_4$ under the following conditions: TR temperature of 1,400°C (heating under nitrogen with a ramp of 15°C/min), WS temperature of 1,100°C, dwell time at activation 60 min, steam mole fraction of 8%. To further clarify the mechanisms taking place during the activation process, a commercial Fe_3O_4 powder (CERAC, purity > 99.5) was subjected to the same testing as the mixed spinel materials perviously. This commercial Fe_3O_4 powder was not subjected to prior calcination under air at 1,400°C like all the rest since this would have resulted in its irreversible oxidation to hematite (α-Fe_2O_3)— as corroborated with such in a separate experiment (as follows).

The comparative results are shown in Figure 3. It can be deduced that the first oxygen evolution peak during activation for the two $NiFe_2O_4$ materials, can be attributed to oxygen that was absorbed from the samples during their prior calcination under air where the as-synthesized ferrite absorbs further oxygen from air and becomes "saturated" with oxygen; this peak is absent in the case of the Fe_3O_4 powder that was not subjected to prior calcination under air. This hypothesis is further corroborated from the literature, since similar oxygen evolution curves from commercial spinel ferrites tested in TR-WS experiments without precalcination, exhibited a single oxygen peak during activation at temperature levels in the range 1,250–1,450°C.[24,25] Even without taking into account this first peak, the favorable effect of the Ni cation on the ferrite's thermal reduction is obvious from the comparison of the peaks from the three materials during activation at 1,400°C. Not only the amount of oxygen evolved from the "plain" ferrous ferrite Fe_3O_4 is much less than that evolved from both $NiFe_2O_4$ ferrites, but the subsequent water splitting capability of Fe_3O_4 is minimal as well.

The two $NiFe_2O_4$ materials (SSS and SHS) exhibited almost identical behavior during every process stage with respect to the hydrogen and oxygen concentration profiles as well as to the oxygen evolution temperatures during thermal reduction. This fact indicates that these two synthesis routes (both starting from solid precursor materials) end up to materials with very similar properties.

Postcharacterization

The XRD spectra of the commercial Fe_3O_4 after its calcination under N_2 at 1,400°C —i.e., after its initial thermal reduction—and under air at the same temperature are shown in Figure 4. It is clear that after the thermal reduction under nitrogen, Fe_3O_4 retains its spinel structure. The spinel peaks are shifted to slightly higher diffraction angles due to the evolution of oxygen from the lattice, but there are no traces of FeO formed as it can be seen in the narrower diffraction angle range shown in Figure 4b. This is further confirmed by the absence of melting in the product—the melting point of FeO is 1,370°C, lower than the thermal reduction temperature tested; should the reduced form of the oxide be that of FeO, significant melting would have been observed. It is also obvious from Figure 4 that, as mentioned previously, calcination of the commercial Fe_3O_4 under air at the same temperature and for the same time results in its complete transformation to Fe_2O_3.

The XRD spectra of the SHS-synthesized $NiFe_2O_4$ after the various processing steps (synthesis, oxidation, activation at 1,400°C under N_2 and cyclic WS—TR operation—with

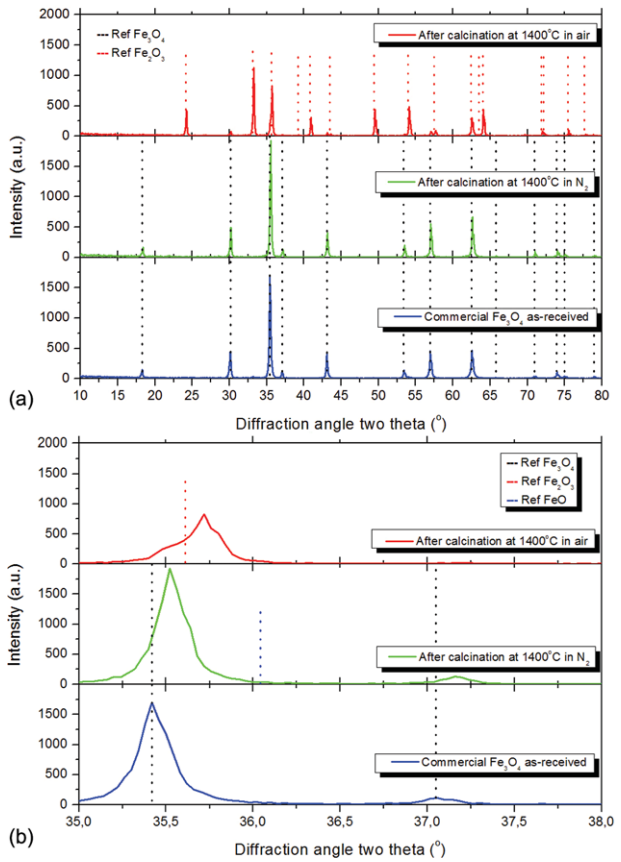

Figure 4. XRD spectra of commercial Fe_3O_4 as-received and after calcination at 1,400°C under nitrogen and under air.

(a) Diffraction angle scale 10–80°, and (b) "magnification" of the diffraction angle scale between 35–38°. [Color figure can be viewed in the online issue, which is available at wileyonlinelibrary.com.]

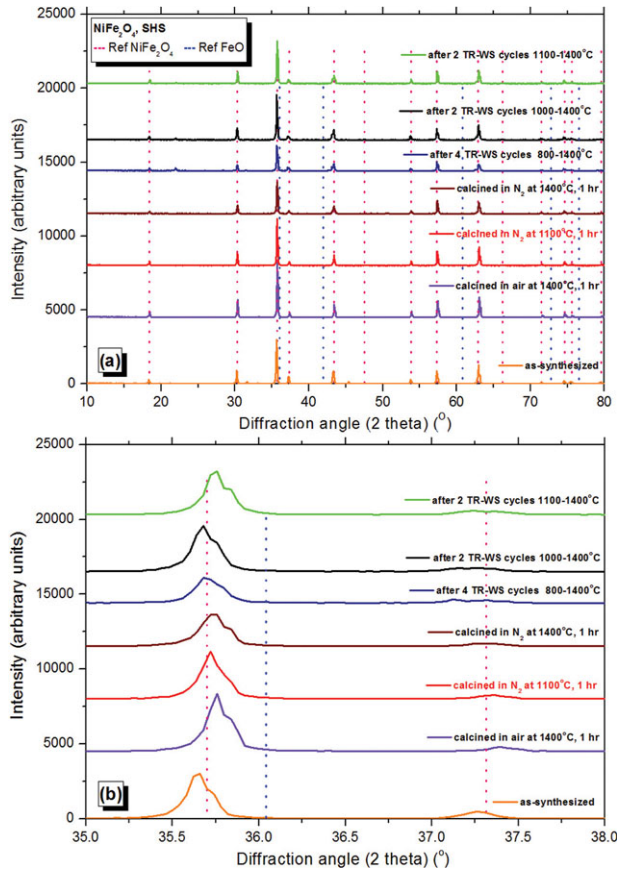

Figure 5. XRD spectra of $NiFe_2O_4$ after all processing steps.

(a) Diffraction angle scale 10–80°, and (b) "magnification" of the diffraction angle scale between 35–38°. [Color figure can be viewed in the online issue, which is available at wileyonlinelibrary.com.]

the last step always being TR) are shown in Figure 5. An experiment involving heating the material under nitrogen but only up to 1,100°C was also performed to "isolate" the material after the completion of the first oxygen evolution peak and investigate any phase differences compared to the material heated under nitrogen at 1,400°C. As mentioned previously,[23] after postsynthesis calcination under air at 1,400°C the product is "oxygen-saturated" single-phase $NiFe_2O_4$ (traces of free Ni that existed in the as-synthesized state have all been oxidized and incorporated in the $NiFe_2O_4$ spinel's lattice). It can be seen in Figure 5 that the material is still, after each process step, single-phase spinel with no other phases having been formed. Even after TR at the highest temperatures tested (1,400°C) there is no evidence of separate divalent metal oxide phase that being either FeO or NiO (Figure 5b where the x-scale is the same with that of Figure 4b for a direct comparison). Thus, it can be concluded that under the temperatures and times tested in this study, the "oxygen-saturated" ferrite is thermally reduced to its "oxygen-deficient" structure $NiFe_2O_{4-\delta}$ and not to FeO or NiO. The only difference among the various process steps is at the relative peaks height: a single calcination of the oxidized powder under nitrogen results in a decrease of the peak height (more intense for the calcination at 1,400°C) due to the observed oxygen loss. Subsequent repetitive exposure at the high WS—TR temperatures (800, 1,000, 1,110, 1,400°C) during the WS—TR cycles induces crystallization of the material accompanied by an increase of the peak height.

The phase evolution of the two $NiFe_2O_4$ materials tested —SHS and SSS—after each process step can be observed in Figure 6 where the XRD spectra of the products are shown within the diffraction angle range 35–38° (same with those of Figures 4b and 5b). The major peak of the SSS material at 800°C coincides as expected, with the reference cubic spinel structure whereas that of the as-synthesized SHS is slightly shifted to lower angles with traces of NiO also present. As already mentioned, most likely, the as-synthesized SHS spinel is an "oxygen-deficient" one since during SHS the spinel has not "absorbed" all oxygen possible due to the very short synthesis time. Postsynthesis calcination under air at 1,400°C "restores" the lattice to a spinel "saturated" with oxygen. After this calcination under air at 1,400°C the peaks of the two materials seem identical, a fact that explains the similar hydrogen yields observed. This similarity with respect to phase composition is maintained after the two WS—TR cycles. As with Fe_3O_4, the shift of the main spinel peak can be noticed after each processing step, due to the distortion of the spinel structure from cubic to tetragonal as oxygen is evolved.

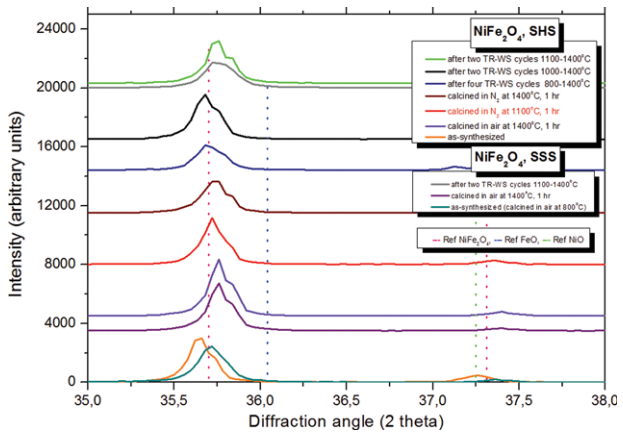

Figure 6. XRD spectra of SHS and SSS $NiFe_2O_4$ after all processing steps in the diffraction angle range 35–38°.

[Color figure can be viewed in the online issue, which is available at wileyonlinelibrary.com.]

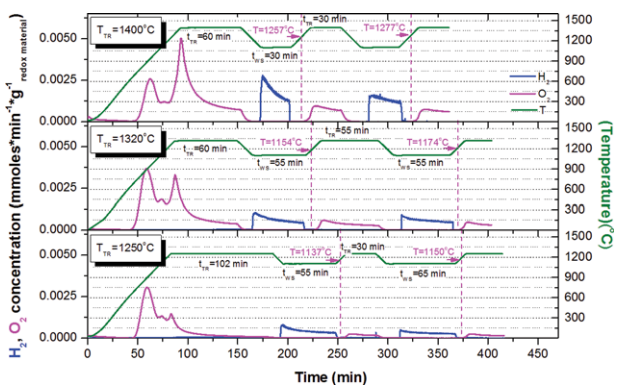

Figure 7. Effect of thermal reduction temperature on hydrogen and oxygen concentration for $NiFe_2O_4$ for water splitting temperature 1,100°C.

[Color figure can be viewed in the online issue, which is available at wileyonlinelibrary.com.]

Effect of thermal reduction temperature

The effect of the TR temperature on the hydrogen and oxygen concentrations is shown for the SHS $NiFe_2O_4$ in Figure 7 for three TR temperatures 1,250, 1,320 and 1,400°C, steam mole fraction of 8% and constant WS temperature of 1,100°C. The last value was selected from the first set of experiments since hydrogen production was maximized at this temperature. It can be very clearly seen that the concentration profiles of both hydrogen and oxygen retain a similar shape regardless of either the TR temperature or the cycle number. The dwell time at the activation temperature was increased from the highest to the lowest activation temperature in an effort to achieve the maximum possible oxygen evolution, i.e., an oxygen final concentration close to zero. This was practically achieved only at the activation temperature of 1,250°C for a dwell time of 102 min. For the same reason the dwell time of the WS and the TR steps was increased in the experiments at TR temperatures of 1,320 and 1,250°C; however, in none of these steps this dwell time was proved long enough for the concentration of the evolved gas to drop to zero.

It is clear that the oxygen liberated during the first, activation step decreases with decreasing activation temperature. This has as an effect that the hydrogen produced during the subsequent WS step—at the same WS temperature of 1,100°C— also decreases with decreasing TR temperature (Figure 7). The oxygen concentration peak corresponding to the lower temperature (i.e., around 883°C) is more or less common in all three experiments, however the oxygen liberated during the constant-high-temperature stage of activation depends strongly on the final TR temperature value. Another observation from Figure 7 is that during the two TR steps the temperature where oxygen evolution starts increases with increasing TR temperature. This point indicates that the material exhibits sintering at the higher temperatures which delays the production of oxygen; the higher the initial activation temperature, the higher the temperature where oxygen starts to be produced during the subsequent TR step.

The important conclusion from this set of experiments is that the maximum oxygen storage capacity of a particular redox material depends strongly on its thermal reduction temperature. For instance, if excessively high thermal reduction temperatures are to be avoided, from the results shown in Figure 7 for $NiFe_2O_4$ one may conclude that since oxygen starts to evolve at a particular "lower" temperature (e.g., of the order of 1,260–1,280°C) then a thermal reduction step performed at this temperature level for a longer dwell time will suffice to thermally reduce the material. The problem with this approach is that the reduced state corresponding to this TR temperature is one that has not "given away" the maximum quantity of oxygen possible (should the thermal reduction be performed at a higher temperature, more oxygen would be released). As a result the hydrogen yield obtained during the subsequent water splitting step is much lower than the one that could be obtained if higher thermal reduction temperatures were employed, as the results in Figure 7 indicate. Thus, to achieve high hydrogen yields, high values of both water splitting and thermal reduction temperatures are required. It can be concluded that at TR temperatures lower than 1,400°C the $NiFe_2O_4$ material has not "given away" the maximum quantity of oxygen possible; this also cannot be assured even for the maximum TR temperature of 1,400°C tested in this work.

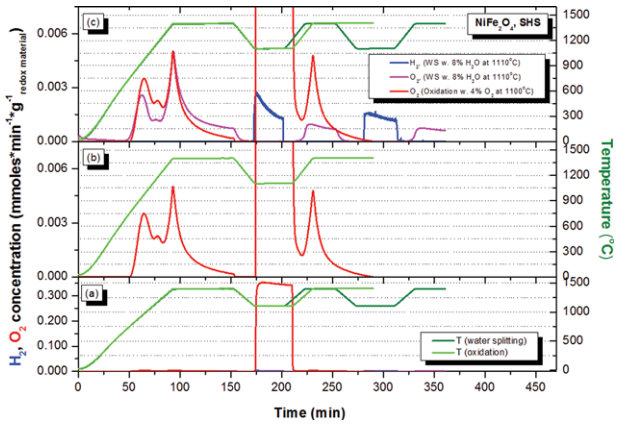

Figure 8. Oxidation at 1,100°C with 4% O_2 in N_2.

(a) "Full-scale" oxygen concentration profile during the experiment, (b) "magnification" of (a) with *y*-axis scaled to the oxygen peak height during activation, and (c) comparison of oxygen concentration evolution between water splitting with 8% steam and oxidation with 4% O_2 in N_2 (water splitting/oxidation—thermal reduction levels of 1,100–1,400°C, respectively, activation dwell time 60 min). [Color figure can be viewed in the online issue, which is available at wileyonline library.com.]

As mentioned previously,[23] by inspection, the amount of hydrogen evolved in the first WS step is much less than double of the amount of oxygen evolved during the activation step (even without including the first oxygen peak). This implies at first that the oxygen deficiency of the reduced ferrite after the activation step is not replenished in full by the oxygen abstracted from steam during the subsequent WS step. In other words, only a part of the oxygen vacancies occurring during activation is filled with oxygen coming from steam during water splitting—at least within the reaction times employed in this study. To corroborate this observation the following experiment was performed: the same SHS $NiFe_2O_4$ material precalcined at 1,400°C was again subjected first to an activation step similar to the aforementioned (calcination under N_2, dwell at 1,400°C for 60 min); then it was cooled to 1,100°C under N_2 where it was exposed to a mixture of 4% O_2 in N_2 for 30 min. In other words, the oxidation of the reduced ferrite was performed with O_2 instead of steam (the percentage of 4% O_2 was selected so that the amount of oxygen in the gas phase to be the same as in the case of oxidation with 8% steam in N_2). Then a TR step was performed, as before, by heating the powder under N_2 to 1,400°C, and a dwell time at 1,400°C of 30 min. The oxygen evolution profile from this experiment is compared to that from the oxidation with 8% steam in Figure 8. In Figure 8a the oxygen concentration during the whole experiment is shown in full-scale (where a minor drop of the oxygen concentration during the oxidation step can be observed, but due to the high level of oxygen concentration a quantitative estimate of the oxygen absorbed during oxidation cannot be made). Figure 8b and 8c are "magnifications" at oxygen concentration levels encountered during activation and water splitting/oxidation. It can be clearly seen (Figure 8b) that the oxygen evolution during the TR step after the oxidation with 4% O_2 is almost an exact replicate—both in height and in shape—of the second oxygen peak observed during activation. This means that the TR process in the

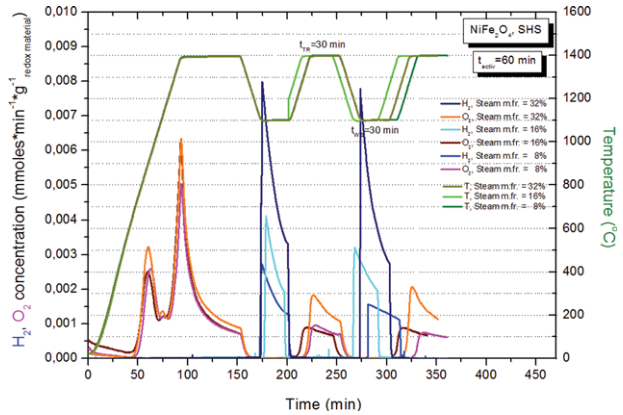

Figure 9. $NiFe_2O_4$, SHS: Effect of steam mole fraction on hydrogen and oxygen concentration evolution; water splitting— thermal reduction levels of 1,100–1,400°C, respectively, activation dwell time 60 min.

[Color figure can be viewed in the online issue, which is available at wileyonlinelibrary.com.]

temperature range 1,100–1,400°C is completely reproducible when the oxidation is performed with oxygen: the oxygen absorbed during this oxidation is evolved in full during the subsequent thermal reduction step in the same way and temperature range where it was evolved during the initial activation stage (Figure 8b). Compared to the respective activation-WS—TR experiment (Figure 8c) it can be seen that the rate of oxygen desorption is much faster in the case of oxygen abstracted from the 4% O_2 mixture than that of the oxygen abstracted from steam. In addition, the difference in the areas under the two oxygen concentration curves—from oxidation with O_2 and from WS—during the TD step at 1,100°C shows that the redox material did not abstract from steam the same amount of oxygen with that abstracted from the 4% O_2 mixture— one reason might being that the WS reaction was not given enough time for completion. In other words, the area under the curve during TR from the oxidation with 4% O_2 shows the "upper" limit of possible oxygen evolution at the particular TR temperature; whether this upper limit can be reached with oxygen abstracted from steam has to be determined from experiments at longer times that will allow for full exhaustion of the gas hydrogen/oxygen products (see the following discussion).

Effect of steam mole fraction

The effect of the steam mole fraction on the hydrogen and oxygen concentration between a TR temperature of 1,400°C and a WS temperature of 1,100°C is shown for the SHS $NiFe_2O_4$ in Figure 9 for three values of the steam mole fraction 8, 16 and 32%. In this set of experiments the activation time was set to 60 min and the dwell times for both the TR and the WS steps to 30 min. The values of the initial rates of hydrogen production, i.e., the maximum values of the hydrogen concentration curves are listed in Table 1 from where it can be considered—at least as a first approximation—that the initial rate of hydrogen production increases almost linearly with increasing steam mole fraction, and, thus, the reaction can be considered as first-order with respect to steam concentration. This point is discussed in detail in the following section devoted to modeling.

Calculations of hydrogen/oxygen yield

As already mentioned, all the WS—TR experiments were terminated before completion since the time required for either the hydrogen or oxygen concentration to drop back to zero would have been impractically long. Therefore, the relevant oxygen/hydrogen concentration curves are "truncated" and the areas under these curves that give the total amount of hydrogen/oxygen moles produced per each reaction step, do not correspond to the maximum possible quantities of hydrogen/oxygen that could be produced under the specific conditions. Nevertheless the total measured hydrogen/oxygen yields (mmol of H_2/O_2 produced per g of redox material) were calculated for each experiment and are summarized in Table 2 and in Figure 10 (in the cases where the dwell time of either the WS or the TR step were different than 30 min, the yields for the first 30 min are listed in Table 2 and plotted in Figure 10 for a direct, objective comparison).

With the exception of one experiment (activation temperature 1,250°C and dwell time 102 min) the dwell time at the activation stage was not enough for oxygen concentration to reach a value close to zero. Therefore, during activation, the redox material did not give away the maximum quantity of oxygen possible at the specific activation temperature. As a result, there is really no means to distinguish which part of the oxygen produced during the next two thermal reduction steps is due to the oxygen abstracted from water during the previous water splitting step, and which part is due to the "continuation" of the thermal reduction process that was "interrupted" before completion during the activation stage (i.e., is oxygen that pre-existed in the redox material before the introduction of steam). Given that the ratio of (hydrogen produced during the WS step)/(oxygen produced during the TR step) does not have to be equal to 2:1 as predicted by the WS reaction stoichiometry. Another reason for discrepancy from the 2:1 ratio is that the two reactions are not equally fast, so the amount of the one gas produced in, for instance, 30 min does not necessarily have to be in stoichiometric analogy to the amount of the other gas produced in the same time. The "efficiency" of the TR process—i.e., the percentage of oxygen abstracted from water that is subsequently released at each particular TR temperature—can be accurately determined only from experiments where the initial activation step lasts until the oxygen concentration curve reaches a zero value; thus, any oxygen that will be produced during subsequent TR steps at the same temperature is safely attributed to that absorbed from steam.

With this rationale and based on the aforementioned findings with respect to the experimental conditions maximizing the gas product yield at each step, an additional set of

Table 1. Maximum Hydrogen Production Rates for SHS $NiFe_2O_4$ as a Function of Steam Mole Fraction (Activation/Thermal Reduction Temperature 1,400°C, Water Splitting Temperature 1,100°C, Dwell Time at Activation 60 min)

Steam mole fraction (%)	Ratio of steam mole fraction	Maximum hydrogen production rate (mmoles H_2/min*g of redox material)		Ratio of maximum hydrogen production rate	
		1st step	2nd step	1st step	2nd step
8	1	0.00280	0.00164	1.00	1.00
16	2	0.00428	0.00369	1.53	2.25
32	4	0.00834	0.00837	2.98	5.10

Table 2. Measured O_2/H_2 Produced (mmol/g of Redox Material) During the First 30 min per Material and per Process Step

Redox material	Steam mole fraction	Activation time	WS-TR T (°C)	mmoles of gas/g of redox material				mmoles of gas/g of redox material		
				Activation	1st WS	1st TR	Ratio H_2/O_2	2nd WS	2nd TR	Ratio H_2/O_2
$NiFe_2O_4$ (SHS)	8 %	30 min	1400-700	0.146	0.016	0.026	0.615	0.022	0.018	1.222
	8 %	30 min	1400-800	0.131	0.028	0.020	1.400	0.017	0.011	1.545
	8 %	30 min	1400-1000	0.125	0.067	0.024	2.792	0.068	0.017	4.000
	8 %	30 min	1400-1100	0.073	0.069	0.014	4.928	0.068	0.011	6.182
	8 %	60 min	1320-1100	0.145	0.023	0.013	1.769	0.020	0.011	1.818
	8 %	102 min	1250-1100	0.084	0.016	0.006	2.666	0.010	0.005	2.000
	8 %	60 min	1400-1100	0.169	0.053	0.020	2.650	0.041	0.017	2.412
	16 %	60 min	1400-1100	0.189	0.071	0.021	3.381	0.064	0.021	3.048
	32 %	60 min	1400-1100	0.209	0.140	0.035	4.000	0.132	0.039	3.385
$NiFe_2O_4$ (SSS)	8 %	60 min	1400-1100	0.203	0.043	0.021	2.048	0.041	0.019	2.158

experiments was performed consisting of one activation and two full WS—TR cycles under the following conditions: TR temperature of 1,400°C, WS temperature of 1,100°C, steam mole fraction of 32%. In this experimental set, the dwell times at each step were extended significantly (in the range of few hours each) until a point where the gas product (either oxygen or hydrogen) concentration curve reached an (almost) zero value (taking into account the practical time limitations on performing these experiments in the laboratory). The respective concentration evolution profiles are shown in Figure 11, where also the total mmoles of gas produced/g of redox material at each process step, as calculated from the area under the respective concentration curve, is reported. A very interesting feature revealed from these experiments is the observation that the ratios of hydrogen to oxygen produced at the two steps of the two WS—TR cycles are very close to the stoichiometric analogy 2:1: 1.98 and 2.25, respectively. This observation also explains any deviations from full-reversibility between the WS and the TR steps of a cycle observed for experiments that did not last until completion. The nonreversibility in the present experiments is due to the fact that the two steps of the cycle occur for fixed time intervals without accounting for the balance between oxygen entering and leaving the redox material, leading to continuous evolution of the amount of oxygen in the redox material This amount affects the rate of the process so in case of "unbalanced" cycles it is not sure that convergence to a steady state will be achieved even after many cycles. On the other hand for balanced cycles (i.e., such that the time intervals of WS and TR are such that the molar ratio of produced H_2 and O_2 to be 2:1) the steady

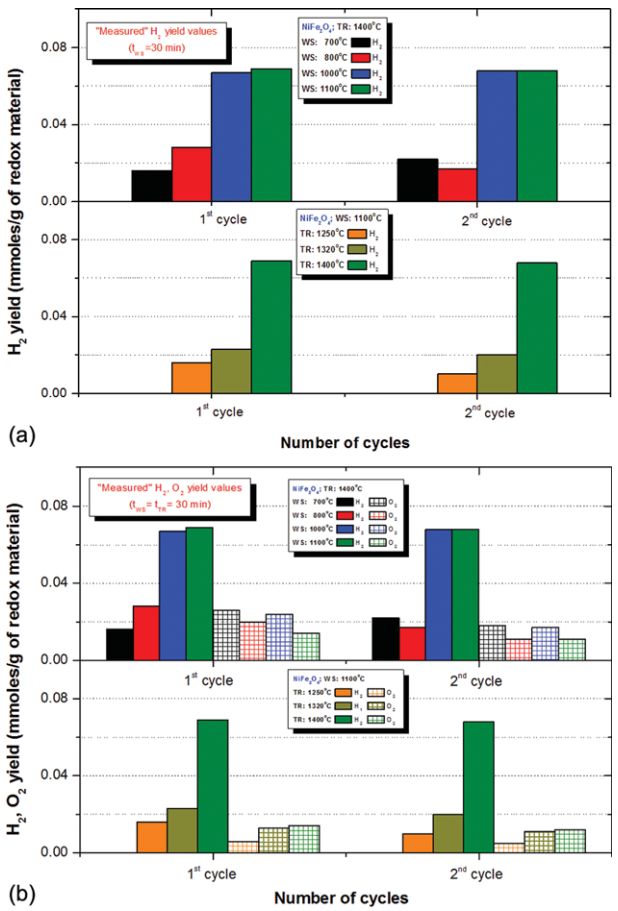

Figure 10. (a) Measured hydrogen yields (mmol of H_2 per g of redox material) during the 30 min time of the water splitting experiments, and (b) comparison to the respective measured oxygen yields (mmol of O_2 per g of redox material) during the 30 min time of the thermal reduction experiments.

[Color figure can be viewed in the online issue, which is available at wileyonlinelibrary.com.]

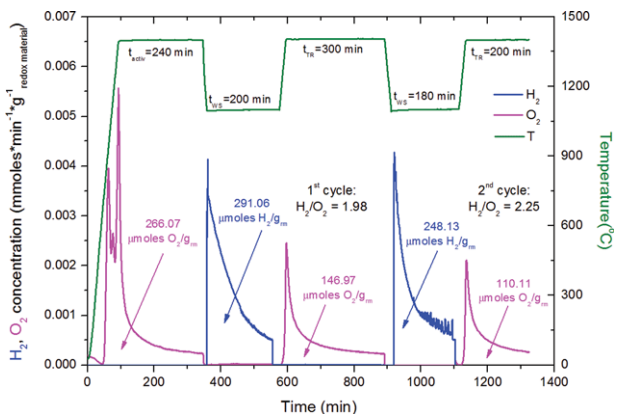

Figure 11. Effect of reaction duration on hydrogen and oxygen concentration and yield for SHS $NiFe_2O_4$; activation and thermal reduction temperature 1,400°C, water splitting temperature 1,100°C, steam mole fraction 32%.

[Color figure can be viewed in the online issue, which is available at wileyonlinelibrary.com.]

state appears from the first cycle as it is evident from Figure 11. Further such experiments are scheduled next, together with parametric experiments with $CoFe_2O_4$ to quantitatively compare the two materials and generalize the reaction mechanisms discussed later.

From the values reported in Table 2, it can be concluded that the hydrogen yields in this study varied within an order of magnitude (0.016–0.140 mmol/g of redox material) depending on the testing conditions. The maximum value of 0.140 mmol H_2/g of redox material (for a WS reaction time of 30 min) was achieved for a WS temperature of 1,100°C, a TR temperature of 1,400°C and a steam mole fraction of 32%. This value is agreement with similar hydrogen yield values reported in the literature for $NiFe_2O_4$, e.g., 0.186 mmol H_2/g of redox material,[25] and 0.4 mmol H_2/g of redox material,[27] taking into account differences among the various studies with respect to steam mole fraction, WS/TR temperatures and duration of the water splitting step. As shown in Figure 11, under the same temperature and steam mole fraction conditions, hydrogen yields can increase from 0.140 to 0.248–0.291 mmol/g of redox material by extending the reaction times.

Modeling–derivation of kinetics

The hydrogen/oxygen concentration evolution profiles are very informative and can be employed to obtain significant information from their shape. In addition, they can be used to determine the kinetics of the water-splitting/thermal reduction reactions from the simple laboratory reactor experimental setup. These kinetic constants can be subsequently introduced in the detailed models of the solar reactor that are necessary for the design and optimization of its operation strategy. As already argued in previous publications, the conditions in the experimental water splitting—thermal reduction laboratory reactor (low conversions, absence of diffusion limitations) permit to ignore as a first approximation the variation of conversion along the redox material bed and assume the water vapor concentration to be constant and equal to its inlet value. In addition, the low-reaction rate ensures that the heat of reactions is not enough to render the problem nonisothermal. Based on the aforementioned, the reactor can be considered as a differential one and for the water splitting step of the cycle, the following mass balance with respect to hydrogen can be written

$$F_{H_2} = R_{WS} \tag{3}$$

where F_{H_2} is the molar flow rate of hydrogen coming out of the reactor (moles of hydrogen per min) per gram of redox material, and R_{WS} is the water splitting reaction rate in terms of moles of H_2 produced per gram of redox material per minute. The water splitting reaction may be actually consisting of several elementary steps, but the purpose here is not to find the exact mechanism but to determine the simplest overall reaction rate expression that can describe the experimental data. In the literature, an empirical scheme for the water splitting kinetics has been proposed[26] according to which the reaction rate depends on the partial pressures of water and hydrogen and not to the state of the redox material. A much simpler rate with a linear dependence on the water concentration has also been proposed.[29] The most general approach to the kinetics is based on finding candidate kinetic expressions from the extensive list referred to gas-solid reactions.[30,31] The simplest choice is to assume a reaction rate (i.e., a hydrogen production rate) of n-th order with respect to vapor concentration C_{H_2O}, and first-order with respect to the empty oxygen storage sites on the surface of the redox material (unimolecular decay law in gas-solid reactions terminology)

$$R_{WS} = k_{WS}\Psi(1-y)C_{H_2O}^n \tag{4}$$

where k_{WS} is the temperature-dependent rate constant (units: m^3/moles/min) of the water splitting reaction, and Ψ is the maximum oxygen storage capacity of the redox material (expressed in moles H_2 produced per g of redox material). Finally, y is the instantaneous actual storage normalized by the maximum one and takes values between 0 and 1. The quantity $(1-y)$ is proportional to the number of empty sites for oxygen storage on the redox material. It is noted that the exponent n can take in general values from 0 to 1 depending on the dominant step in WS reaction. For the range of vapor concentration experiments performed here it was found that the exponent is close to 1 implying that the WS process is dominated by the vapor adsorption to the redox material step (Table 1). It is noted that the reaction mechanism proposed here is not expected to be able to describe the complete redox kinetics. It is just a fundamental mechanism describing the reaction of the surface layers of the redox material. Phenomena such as reaction in the bulk material and associated oxygen transport kinetics are not considered. Nevertheless, the deviations between the simple model and the experimental data are expected to suggest how to incorporate these phenomena in the model.

Thus, the hydrogen mass balance in the bed takes the form

$$F_{H_2} = k_{WS}\Psi(1-y)C_{H_2O} \tag{5}$$

The dynamics of the storage sites on the redox material leads to the equation

$$\Psi\frac{dy}{dt} = R_{WS} = k_{WS}\Psi(1-y)C_{H_2O} \tag{6}$$

We introduce at this point a new variable ϕ which it is defined as

$$\phi = \Psi(1-y) \tag{7}$$

i.e., ϕ it is the instantaneous capacity of water splitting of the redox material (in moles of produced hydrogen per g of redox material). In this way, the two variables y and Ψ are replaced by the variable ϕ, eliminating the theoretical quantity Ψ which may be inaccessible in practice (at least for the experimental reaction times of this work). The quantity ϕ can be considered as the instantaneous "driving force" for the reaction. Such a simplification is possible only in the case of a linear relation between R_{WS} and y as the one described in Eq. 4. Replacing ϕ in Eq. 5 leads to

$$\frac{d\phi}{dt} = -k_{WS}\phi C_{H_2O} \tag{8}$$

from which we obtain

$$\phi = \phi_0 e^{-k_{WS}C_{H_2O}t} \tag{9}$$

where ϕ_0 is the value of φ at the beginning of each water splitting cycle. Substitution of 9 and of definition in Eq. 5 leads to

$$F_{H_2} = k_{WS} C_{H_2O} \phi_0 e^{-k_{WS} C_{H_2O} t} \tag{10}$$

This is the final working equation to be used to extract the temperature-dependent parameters k_{WS} and ϕ_0 from the experimental curves. The procedure is as follows:

1. Each hydrogen concentration evolution profile—as obtained from the mass spectrometer in units of moles (or mmol) of hydrogen per min— is fitted with an exponential decay function of the form $y = ae^{(-bt)}$ from where a and b are calculated;

2. From the relationship $b = -k_{WS} C_{H_2O}$ (C_{H_2O} is the vapor concentration and can be calculated at the water splitting temperature of each experiment) k_{WS} can be calculated;

3. From the relationship $a = k_{WS} C_{H_2O} \phi_0$ (with C_{H_2O}. calculated as earlier, and k_{WS} already calculated from step 2 above, ϕ_0 can be calculated also.

Thus, we can obtain values for the constants k_{WS} and ϕ_0 from each WS step of the cycle performed at each water splitting temperature.

Similarly, for the thermal reduction (regeneration) step, the starting equation is the mass balance for oxygen

$$F_{O_2} = R_{TR} \tag{11}$$

where F_{O_2} is the molar flow rate of oxygen coming out of the reactor (moles of oxygen per minute) per g of redox material, and R_{TR} is the thermal reduction reaction rate in terms of moles of O_2 produced per g of redox material per minute. A simple first-order expression for the reaction rate is

$$R_{TR} = k_{TR} \psi \tag{12}$$

where ψ is the instantaneous concentration of adsorbed oxygen (moles of O_2 per gram of redox material). The variables ψ, Ψ, and y are related by

$$\psi = \Psi y / 2 \tag{13}$$

$$\frac{d\psi}{dt} = -k_{TR} \psi \tag{14}$$

$$\psi = \psi_0 e^{-k_{TR} t} \tag{15}$$

where ψ_0 is the initial value of ψ at the beginning of the thermal reduction step. Substitution of (15) in (11) leads to

$$F_{o_2} = k_{TR} \psi_0 e^{-k_{TR} t} \tag{16}$$

which is the working equation for the analysis of the experimental data of the thermal reduction step and can be used, similarly to the procedure for water splitting, to extract the temperature-dependent parameters k_{TR} and ψ_0 from the experimental oxygen concentration evolution curves. The procedure is again as follows:

1. each oxygen concentration evolution profile is fitted with an exponential decay function of the form $y = ae^{(-bt)}$ from where a and b are calculated;

2. from the relationship $b = -k_{TR}$, k_{TR} is calculated

3. from the relationship $a = k_{TR} \psi_0$ and k_{TR} already calculated from step 2, ψ_0 can be calculated also.

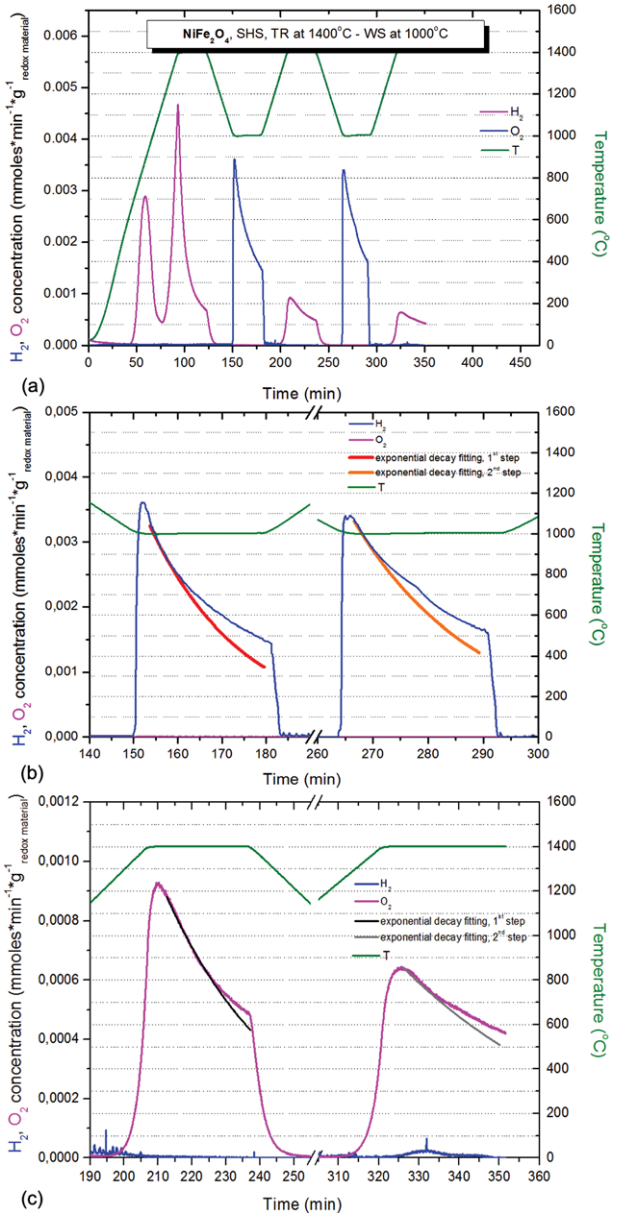

Figure 12. $NiFe_2O_4$, SHS, activation and thermal reduction temperature 1,400°C, water splitting temperature 1,000°C.

(a) Experimental oxygen/hydrogen concentration profiles during the whole cycle; (b) and (c) magnification of the water splitting/thermal reduction steps and fitting curves for hydrogen/oxygen concentration, respectively. [Color figure can be viewed in the online issue, which is available at wileyonlinelibrary.com.]

Thus, we can also obtain values for the constants k_{TR} and ψ_0 (from each TR step of the cycle performed at each thermal reduction temperature).

Equations 10 and 16 were employed to fit the experimental hydrogen/oxygen concentration evolution profiles, respectively, and extract the respective kinetic parameters for the case of $NiFe_2O_4$. It should be mentioned that only the part of the hydrogen/oxygen concentration profiles after their respective peaks (exponential-like decay) should be and was included in the fitting procedure. Ideally, the product gas (hydrogen/oxygen) concentration should reach instantaneously its highest value and thereafter decrease. However, in

Table 3. Calculated Kinetic Constants for the Water Splitting and the Thermal Reduction Reaction of SHS $NiFe_2O_4$

Experiments with varying WS temperature and constant TR temperature					
Cycle step	ϕ_0 (mmoles/g redox)	k_{WS} (m^3/min*mole)		k_{TR} (1/min)	Ψ_0 (mmoles/g redox)
WS	700		TR	1400	
1st	0,012	0,0814	1st	0,0297	
2nd	0,014	0,0897	2nd		
WS	800		TR	1400	
1st	0,028	0,0599	1st		
2nd			2nd	0,0194	0,023
3rd	0,400	0,0454	3rd	0,0561	0,018
4th	0,464	0,0504	4th	0,0165	0,036
WS	1000		TR	1400	
1st	0,067	0,0565	1st	0,0290	0,030
2nd	0,072	0,0538	2nd	0,0196	0,036
WS	1100		TR	1400	
1st	0,072	0,0694	1st	0,0532	0,010
2nd	0,076	0,0549	2nd	0,0222	

Experiments with varying TR temperature and constant WS temperature					
Cycle step	ϕ_0 (mmoles/g redox)	k_{WS} m^3/min*mole)		k_{TR} 1/min)	Ψ_0 (mmoles/g redox)
WS	1100		TR	1250	
1st	0,019	0,0514	1st	0,0198	0,012
2nd	0,023	0,0226	2nd	0,0229	0,010
WS	1100		TR	1320	
1st	0,038	0,0324	1st	0,0301	0,019
2nd	0,047	0,0218	2nd	0,0274	0,016
WS	1100		TR	1400	
1st	0,072	0,0694	1st	0,0532	0,010
2nd	0,076	0,0549	2nd	0,0274	0,016

the experimental configuration the diffusion of the evolved gas in the line to the mass spectrometer has as a result the gradual increase of the measured product gas concentration from zero to its maximum value. Indeed, the time interval required for hydrogen concentration to reach its highest value is characteristically around 50–100 s for all the experiments, regardless of the materials composition. If the gradual rise of hydrogen productions was due to a physical mechanism on the redox materials' surface its duration would be expected to be material-dependent.

Typical comparisons between the fitting and the actual experimental hydrogen and oxygen gas concentration evolution curves are shown in Figure 12 for the case corresponding to thermal reduction at 1,400°C and water splitting at 1,000°C; similar results were obtained for practically the whole set of experiments. In Figure 12a, the whole experiment consisting of one activation and two water splitting/thermal reduction steps is shown. Figure 12b shows a magnification of the two hydrogen production peaks, and Figure 12c the respective magnification of the oxygen production peaks, which were subsequently fitted with an exponential-decay function $y = ae^{(-bt)}$ (red/orange and black/gray curves for the first/second step, respectively).

With respect to the hydrogen concentration profiles it can be observed that, the fitting curve lies significantly underneath the actual experimental curve (Figure 12b). This means that the simple first-order reaction rates employed here can describe adequately only the first part of the experimental hydrogen evolution curves. This part corresponds to a reduction of the initial reaction rate of about 30%. In other words, the linear theory (Eq. 4) predicts smaller reaction rates at higher reaction times than the experimental ones. This implies that the number of the active surface sites of the redox material is not reduced in accordance to the reaction rate. A possible explanation is that slow transfer of adsorbed oxygen molecules takes place from surface sites to another region of the redox material not initially directly accessible by the gas phase (steam). In this way the number of the surface empty sites is not reduced very fast (as fast as predicted by Eq. 4), and the reaction is sustained as suggested by the experimental results. In other words, perhaps more than one "population" of oxygen storage sites participate in the water splitting reaction as this is evolving. The same trend— i.e., underprediction of the gas evolution rate by the linear theory, even though to a lesser extent —can be also observed in the oxygen concentration profiles (Figure 12c). This suggests that more complicated reaction models taking into account the structure of the redox material are needed to describe the whole extent of the experimental data. At this point no attempt can be made to simulate the second part of the curve even using the phenomenological gas-solid reaction kinetic laws because in any case (except the linear rate law used here) the total reaction capacity must be explicitly known. The linear reaction model is the only one for which the reaction rate depends only on the instantaneous state of the material and on no other parameter like Ψ. To extent the reaction model of this work, the whole experimental hydrogen/oxygen concentration evolution curves up to the exhaustion of the storage sites are required; such experiments are scheduled as the next part of the work. Nevertheless, the first-order model employed here is appropriate for the description of the dynamics of the surface adsorbed oxygen, being an important part of the whole redox system dynamics.

The results of the analysis with respect to the calculation of the kinetic parameters are summarized in Table 3 (the omission of some results is due to the fact that the fitting was poor for the particular step/experiment, not leading to reliable calculations). With respect to the water splitting reaction, it can be observed that the values of the rate

constant are of the same order at each experiment and do not seem to depend strongly on the water splitting reaction temperature. This fact, taking into account the rather large water splitting temperature range spanned (700–1,100°C), does not seem to correspond to an Arrhenius-type temperature dependence of k_{WS}. In addition, the dependence of k_{WS} on the initial activation temperature does not seem to be so strong either. This is an indication that the rate-controlling step during water splitting perhaps is not a chemical reaction *per se* (depending exponentially on temperature), but rather another elementary step (e.g., adsorption-like), much less strongly temperature-dependent.

The values obtained for k_{TR} for the thermal decomposition step (oxygen release) suffer from more scattering. With respect to the values provided in the upper half of Table 3 (from experiments with varying WS temperature and constant TR temperature), a trend of with respect to the (previous) water splitting temperature cannot be established. On the contrary, from the results in the lower half of Table 3 (from experiments with varying TR temperature and constant WS temperature) it appears that k_{TR} increases with increasing activation (thermal reduction) temperature, but some more experiments are needed to quantify this trend through the estimation of the activation energy of the reaction. Despite the large scatter of the kinetic constant values between cycles one could say that (1) there is not a specific pattern of WS temperature influence on k_{TR}, and (2) k_{TR} increases with the TR temperature. Both observations are compatible with expectations based on the existing picture of the process.

The calculated values of ϕ_0—which is the instantaneous capacity of water splitting of the redox material at the beginning of each water splitting cycle, expressed in moles of produced hydrogen per g of redox material—are increasing with an increase of both the water splitting temperature as well as the activation/thermal reduction temperature. However, it is not a fundamental quantity; it just refers to the start of each WS cycle and depends on the history of the redox material treatment (initial activation and WS, TR cycles). The unexpectedly high values of observed in the third and fourth steps of the cycle between 1,400 and 800°C (in red) are due to the grinding that took place before the third step which had as an effect the modification of the structure of the redox material and the enhancement of the surface area directly accessible for oxygen adsorption from the gas phase.

Conclusions

Cyclic thermal reduction—water splitting parametric experiments with in-house synthesized $NiFe_2O_4$ powders were performed to quantify the effects of operational parameters on hydrogen and oxygen yields and extract the kinetic data of the water splitting and thermal reduction reactions. It was determined that hydrogen yield depends on both thermal reduction as well as water splitting temperature. High-thermal reduction temperature has, as a result, the evolution of higher quantities of oxygen and the consequent production of higher quantities of hydrogen during the subsequent water splitting steps. For constant thermal reduction temperature, the quantity of hydrogen produced increases with increasing water splitting temperature with a drastic increase of hydrogen yield taking place between 800 and 1,000°C; however, the yield seems to reach a "plateau" value in the temperature range 1,000–1,100°C.

During this cyclic operation and after the thermal reduction stage, there was no evidence of formation of the divalent iron oxides (wüstite/FeO or NiO); the material remained single-phase spinel practically during the whole cyclic operation, however with different oxygen content after each step. To induce water splitting capability on the material, an initial "oxygen deficiency" has to be caused on it (by thermal reduction under inert atmosphere). However, this oxygen deficiency is not "fully" exploited during the subsequent water splitting step; only a part of the empty oxygen sites is occupied by oxygen abstracted from water during water splitting (at least within the water splitting temperature range tested in this study).

The experiments with varying steam mole fraction performed showed that the water splitting reaction can as a first approximation considered first-order with respect to steam concentration. Models linear with respect to the number of oxygen storage sites were proposed for both WS and TR reactions. It was found that this linear model follows the experimental hydrogen production reaction rate up to a reduction of about 30% of its initial value. After this point, the experimental rate sustains higher values than those predicted by the model, implying a variation of the reaction mechanism (probably the reaction continues in internal oxygen storage sites where the oxygen is transferred through solid-state diffusion). Further modeling of the reaction kinetics requires the complete hydrogen/oxygen production reaction rate curves up to the exhaustion of the gas products.

The calculation of kinetic constants for the water splitting reaction has resulted in a very weak temperature dependence in the temperature region 700–1,100°C studied in this work. This fact indicates that perhaps the rate-controlling step is not a chemical reaction *per se* (for which an Arrhenius-type temperature dependence would be expected), but rather another less strongly temperature-dependent step like the adsorption of steam molecules on the redox material's surface. This assertion is compatible to the linear dependences of the reaction rate from steam concentration and oxygen storage sites. Regarding the thermal reduction kinetic constant, it is shown that there is no influence by the WS reaction temperature and there is an increase as the TR temperature increases. A complete picture of the WS—TR process has been revealed based on the findings of this work and specific ways to further quantify the process are set forth.

As previously mentioned, this work is focused on the development of "refined" kinetic models, taking into account these experimental findings; e.g., incorporating various oxygen storage sites populations. This analytical work is scheduled to be complemented by experiments at longer activation—water splitting—thermal reduction times as well as with experiments with $CoFe_2O_4$ to verify and generalize the trends observed so far. These "refined" kinetic parameters will then be employed in a single channel reactor model to simulate the hydrogen production in monolithic reactors under different operation strategies and identify the effects of crucial operating parameters.

Acknowledgments

The authors would like to thank the Fuel Cells and Hydrogen Joint Technology Initiative and the European Commission for partial funding of this work within the Collaborative Project "245224-HYDROSOL-3D: Scale Up of Thermochemical Hydrogen Production in a Solar Monolithic Reactor: a 3rd Generation Design Study" under the FCH—JU-2008-1 Call.

Notation

C = gas species concentration, moles of gas/m^3
F = molar gas flow rate, moles of gas per minute per g of redox material
k = temperature-dependent reaction rate constant, m^3/moles/min
R = reaction rate, moles of gas produced per minute per g of redox material
T = absolute temperature, K

Greek letters

Ψ = maximum oxygen storage capacity of the redox material, moles of H_2 produced per g of redox material
ϕ = instantaneous capacity of water splitting of the redox material, moles of H_2 produced per g of redox material
y = instantaneous actual oxygen storage normalized by the maximum one
ψ = instantaneous concentration of adsorbed oxygen, moles of O_2 per g of redox material

Subscripts

H_2 = hydrogen
O_2 = oxygen
WS = water splitting
TR = thermal reduction
0 = initial (at the beginning of the cycle step)

Literature Cited

1. Kodama T. High-temperature solar chemistry for converting solar heat to chemical fuels. *Prog En Comb Sci*. 2003;29(6):567–97.
2. Steinfeld A, Sanders S, Palumbo R. Design aspects of solar thermochemical engineering - A case study: Two-step water-splitting cycle using the Fe_3O_4/FeO redox system. *Solar Energy*. 1999;65(1):43–53.
3. Müller R, Steinfeld A. H_2O-splitting thermochemical cycle based on ZnO/Zn-redox: Quenching the effluents from the ZnO dissociation. *Chem Eng Sci*. 2008;63(1):217–27.
4. Agrafiotis C, Roeb M, Konstandopoulos AG, Nalbandian L, Zaspalis VT, Sattler C, Stobbe P, Steele AM. Solar water splitting for hydrogen production with monolithic reactors. *Solar Energy*. 2005; 79(4):409–21.
5. Roeb M, Sattler C, Klüser R, Monnerie N, deOliveira L, Konstandopoulos AG, Agrafiotis C, Zaspalis VT, Nalbandian L, Stobbe P, Steele AM. Solar hydrogen production by a two-step cycle based on mixed iron oxides. *J Solar Energy Eng*. 2006;128:125–33.
6. Heck RM, Farrauto RJ. *Catalytic Air Pollution Control - Commercial Technology*. New York: Van Nostrand Reinhold; 1995.
7. Agrafiotis CC, Mavroidis I, Konstandopoulos AG, Hoffschmidt B, Stobbe P, Romero M, Fernandez-Quero V. Evaluation of porous silicon carbide monolithic honeycombs as volumetric receivers/collectors of concentrated solar radiation. *J Solar En Mat Solar Cells*. 2007;91:474–88.
8. Kaneko H, Miura T, Fuse A, Ishihara H, Taku S, Fukuzumi H, Naganuma Y, Tamaura Y. Rotary-type solar reactor for solar hydrogen production with two-step water splitting process. *Energy Fuels*. 2007;21:2287–93.
9. Gokon N, Takahashi S, Yamamoto H, Kodama T. Thermochemical two-step water-splitting reactor with internally circulating fluidized bed for thermal reduction of ferrite particles. *Int J Hydrogen Energy*. 2008;33(9):2189–99.
10. Gokon N, Mataga T, Kondo N, Kodama T. Thermochemical two-step water splitting by internally circulating fluidized bed of $NiFe_2O_4$ particles: Successive reaction of thermal-reduction and water-decomposition steps. *Int J Hydrogen Energy*. 2011;36(8):4757–67.
11. Diver RB, Miller JE, Allendorf MD, Siegel NP, Hogan RE. Solar thermochemical water-splitting ferrite-cycle heat engines. *J Solar Energy Eng*. 2008:130:041001–8.
12. Miller JE, Allendorf MD, Diver RB, Evans LR, Siegel NP, Stuecker JN. Metal oxide composites and structures for ultra-high temperature solar thermochemical cycles, *J Mater Sci*. 2008;43:4714–28.
13. Roeb M, Monnerie N, Schmitz M, Sattler C, Konstandopoulos AG, Agrafiotis C, Zaspalis VT, Nalbandian L, Steele AM, Stobbe P. Thermo-chemical production of hydrogen from water by metal oxides fixed on ceramic substrates. Proceedings of the 16th World Hydrogen Energy Conference, Lyon, France, Jun. 13–16, 2006.
14. Agrafiotis CC, Pagkoura C, Lorentzou S, Kostoglou M, Konstandopoulos AG. Hydrogen production in solar reactors. *Catal Today*. 2007;127:265–77.
15. Roeb M, Säck JP, Rietbrock P, Prahl C, Schreiber H, Neises M, Graf D, Ebert M, Reinalter W, Meyer-Grünefeldt M, Sattler C, Lopez A, Vidal A, Elsberg A, Stobbe P, Jones D, Steele A, Lorentzou S, Pagkoura C, Zygogianni A, Agrafiotis C, Konstandopoulos AG. Test operation of a 100-kW pilot plant for solar hydrogen production from water on a solar tower. *Solar Energy*. 2011;85(4):634–44.
16. Siemund S, Leclerc JP, Schweich D, Prigent M, Castagna F. Three-way monolithic converter: simulations versus experiments. *Chem Eng Sci*. 1996;51:3709–20.
17. Dubien C, Schweich D, Mabilon G, Martin B, Prigent M. Three-way catalytic converter modelling: fast- and slow- oxidizing hydrocarbons, inhibiting species, and steam-reforming reaction. *Chem Eng Sci*. 1998;53:471–81.
18. Young LC, Finlayson BA. Mathematical-Models of monolith catalytic-converter. Application to automobile exhaust. *AIChE J*. 1976;22:343–53
19. Roeb M, Neises M, Säck JP, Rietbrock P, Monnerie N, Dersch J, Schmitz M, Sattler C. Operational strategy of a two-step thermochemical process for solar hydrogen production. *Int J Hydrogen Energy*. 2009;34(10):4537–45.
20. Dersch J, Mathijssen A, Roeb M, Sattler C. Modelling of a solar thermal reactor for hydrogen generation. *Modelica*. 2006;441–48.
21. Kostoglou M, Lekkos CP, Konstandopoulos AG. On mathematical modelling of solar hydrogen production in monolithic reactors. *Comp Chem Eng*. 2011;35(9):1915–22.
22. Zygogianni A, Lorentzou S, Pagkoura C, Kostoglou M, Agrafiotis C, Konstandopoulos AG. On the modelling of solar monolithic reactors for hydrogen production. In: Proceedings of 15th International SolarPACES Concentrating Solar Power Symposium. Berlin, Germany, Sept. 15–18, 2009.
23. Agrafiotis C, Pagkoura C, Zygogianni A, Kostoglou M, Konstandopoulos AG. Hydrogen production via solar-aided water splitting thermochemical cycles: Combustion synthesis and preliminary evaluation of spinel redox-pair materials. *Int J Hydrogen Energy*. 2012;37:8964–8980.
24. Fresno F, Fernández-Saavedra R, Gómez-Mancebo MB, Vidal A, Sánchez M, Rucandio MI, Quejido Alberto J, Romero M. Solar hydrogen production by two-step thermochemical cycles: evaluation of the activity of commercial ferrites. *Int J Hydrogen Energy*. 2009;34(7):2918–24.
25. Fresno F, Yoshida T, Gokon N, Fernández-Saavedra R, Kodama T. Comparative study of the activity of nickel ferrites for solar hydrogen production by two-step thermochemical cycles. *Int J Hydrogen Energy*. 2010;35(16):8503–10.
26. Tsuji M, Togawa T, Wada Y, Sano T, Tamaura Y. Kinetic study of the formation of cation-excess magnetite. *J Chem Soc Faraday Trans*. 1995;91:1533–38.
27. Rosmaninho MG, Herreras S, Lago RM, Araujo MH, Navarro RM, Fierro JLG. Effect of the partial substitution of Fe by Ni on the structure and activity of nanocrystalline $NixFe_{3-x}O_4$ ferrites for hydrogen production by two-step water-splitting nanosci. *Nanotechnol Lett*. 2011;3(5):705–716.
28. Kaneko H, Naganuma Y, Tamaura Y. Intermediate formation in the reduction of Ni-ferrite with irradiation of high-flux infrared beam up to 1823 K. *J Phys Chem Solids*. 2012;73:63–72.
29. Chen KS, Hogan RE. A two phase model for solar thermochemical water splitting with FeO/Fe_3O_4. Proceedings of ES2009. 2009 ASME 3rd International Conference of Energy Sustainability. San Francisco, CA, July 19–23, 2009.
30. Francis TM, Lichty PR, Weimer AW. Manganese oxide dissociation kinetics for the Mn_2O_3 thermochemical water-splitting cycle. Part 1: Experimental. *Chem Eng Sci*. 2010;65(12):3709–17.
31. Go KS, Son SR, Kim SD. Reaction kinetics of reduction and oxidation of metal oxides for hydrogen production. *Int J Hydrogen Energy*. 2008;33:5986–95.

Manuscript received Mar. 21, 2012, and revision received Jun. 19, 2012.